Single Molecule Visualizations of Polymer Partitioning within Model Pore Geometries

Dmytro Nykypanchuk,[†] Helmut H. Strey,[‡] and David A. Hoagland*,[†]

Department of Polymer Science and Engineering, University of Massachusetts Amherst, Amherst, Massachusetts 01003, and Department of Biomedical Engineering, Stony Brook University, Stony Brook, New York 11794

Received September 20, 2004; Revised Manuscript Received October 19, 2004

ABSTRACT: Probing the thermodynamics of polymer confinement in small pores, single DNA molecules were imaged by fluorescence microscopy as they partitioned within a pair of adjacent interconnected spherical cavities prepared by the colloidal templating method. This method produces pores of precisely known geometry and controlled level of confinement. As expected, a polymer weakly or moderately confined by cavities of unequal diameter was observed to maximize its configurational entropy by partitioning toward the larger cavity. The polymer's cavity-to-cavity partition coefficient could be derived from the visualized bias in cavity occupation, and segmental excluded volume notably influences how this coefficient depends on chain length and two cavity sizes. A DNA molecule strongly confined within a pair of equal-sized cavities predominately adopts "bridging" configurations, splitting its segments between the two cavities. Segmental excluded-volume stabilizes such configurations; the stability reveals that a chain must overcome a doubly peaked energy barrier to move between cavities.

Introduction

Confining a flexible polymer in a small pore reduces the molecule's configurational entropy. Confronted with a pore space offering different levels of confinement at different locations, such a polymer can maximize its entropy by partitioning to (preferentially occupying) the location or locations where the molecule is able to adopt the largest number of configurations. At equilibrium, partitioning eliminates inhomogeneities of chemical potential by creating inhomogeneites of polymer concentration. Bigger polymers suffer more strongly from partitioning than smaller ones, a trend exploited in many methods that separate polymers by molecular size (gel permeation chromatography, gel electrophoresis). Although the importance of confinement-mediated partitioning is widely appreciated,[1−4] molecular theories for the effect have not been experimentally tested in a systematic series of well-defined pore geometries, and the dynamic partitioning process has not been visualized. Here, we describe real-time, single-molecule imaging of flexible polymers (DNA molecules) partitioned within pore spaces prepared by the colloidal templating method. Our approach provides a quantitative, molecular-level assessment of polymer partitioning and affords many insights into the dynamics of heterogeneously confined polymers.

Equilibrium partitioning of solute between two regions of dissimilar free energy is quantified through the partition coefficient K, the ratio of the two solute concentrations. Porous materials that create spatial variations of free energy for polymeric solutes are usually chosen so that spatial variations of enthalpy are negligible. If so, by picking an unconfined region as the reference state, $K = \exp(\Delta S_c/k)$, where ΔS_c is the confinement entropy and k is the Boltzmann constant. Employing a Gaussian description for a confined chain and allowing the chain to sample equally all configurations not intersecting pore boundaries, Casassa[5] developed the earliest theories of ΔS_c germane to flexible polymers. Analytical results were reported for chains trapped within spherical, cylindrical, and slitlike pores. For a polymer of average end-to-end distance R partitioned into a pore of comparable or smaller size D, a Gaussian chain description leads to a scaling relationship,

$$\Delta S_c \sim N/D^2 \tag{1}$$

where N is the polymer's number of Kuhn segments. Scaling relationships for ΔS_c are extensively discussed in de Gennes.[3]

Several features missing in a Gaussian chain description can significantly influence ΔS_c. In a good solvent, excluded volume effectively precludes overlap of chain segments, and an unconfined flexible polymer responds by swelling. Pore walls frustrate this swelling, thereby increasing $|\Delta S_c|$ from its Gaussian chain value. For chains of finite stiffness/length, confinement models must replace Gaussian chain statistics with wormlike chain statistics.[6−9] Assessed at equal R, $|\Delta S_c|$ for a wormlike chain is usually less than for a Gaussian chain (pore geometry affects the direction of the trend). Finally, nondilute chains in a good solvent feel each other even as they interact with pore walls, and the correlation length of the bulk solution supersedes R as the polymer length governing partitioning. Computational methods, along with more sophisticated scaling approaches, address deficiencies of the Gaussian chain description, and detailed results have been reported for several idealized confinement geometries.[9−15]

Sorption, size exclusion chromatography, and interferometry experiments have all provided average K values for flexible polymers partitioned from solution into bulk materials possessing geometrically ill characterized and/or polydisperse pores.[16−19] For dilute polymer solutions, trends fall roughly in line with predictions derived using the Gaussian chain description. Recently, a conductance method has been applied to the study of polymers partitioned within membrane-

[†] University of Massachusetts Amherst.
[‡] Stony Brook University.
* To whom correspondence should be addressed. E-mail dah@neurotica.pse.umass.edu.

10.1021/ma048062n CCC: $30.25
Published on Web 12/16/2004

Table 1. Experimental Parameters

molecular size (base pairs, bp)	R_{g0} (nm)	D_1 (nm)	D_2 (nm)	K_p
2686	123	1400	920	0.83 ± 0.16
4361	157	608	350	0.01 ± 0.009
4361	157	608	462	0.22 ± 0.11
4361	157	920	608	0.53 ± 0.18
7249	203	1400	608	0.054 ± 0.037
7249	203	920	608	0.095 ± 0.021

bound protein nanopores;[20] systematic variations of the chemistry, geometry, and size of such nanopores are difficult or impossible.

Experimental Section

Well-defined confinement geometries of submicron size were prepared by the colloidal templating method.[21] To prepare such geometries, dispersed polystyrene beads of appropriate diameter(s) were initially deposited on a planar substrate by solvent evaporation. The beads, with diameters from 340 to 1360 nm, were purchased as NIST-traceable size standards (Duke Scientific). To achieve submonolayer coverage (first experiments, with isolated cavity pairs), a bidisperse suspension of highly diluted beads (0.01−0.5 wt %) in ethanol was streaked across a heated (50 °C) glass coverslip. To generate full monolayers (second experiments, with hexagonally packed cavities), an 80:20 ethanol/water suspension of monodisperse beads was allowed to dry on a coverslip at room temperature. After crafting a ~200 μm gap above the bead-coated surface with a second coverslip, a polymerizable fluid, 30 wt % acrylamide:bis(acrylamide) (20:1) in water, was infused around the beads. Following polymerization, the coverslips were gently removed, leaving behind a free-standing hydrogel film decorated on one surface with embedded beads. Each surface contact exposed a small bead area. Thus, by immersing the film in toluene, a solvent for polystyrene, beads were replaced by spherical cavities that opened to the film exterior through small holes. Likewise, small interconnecting holes appeared in the plane of the film where two beads had previously contacted each other.

Imposition of a small electric field (~10 V/cm) perpendicularly across the hydrogel film induced DNA molecules of a bathing solution (40 mM Tris-Acetate buffer at pH 8, 10 mM NaCl, 5 mM sodium ascorbate, 1 mM EDTA) to enter the cavities through the exterior holes. These holes were then sealed with a viscous silicone oil (Fluka silicone oil AP1000), trapping single molecules inside a small fraction (<1%) of templated cavities. The hydrogel matrix is passive to DNA, providing only geometric constraints. Further, since this matrix is uncharged and the Debye length is small (≈2 nm), electrostatic interactions between DNA and matrix are negligible. Prior mixing of the DNA molecules with TOTO-1 (Molelcular Probes), an irreversibly bound fluorescent dye, allowed the trapped molecules to be viewed by fluorescence microscopy (Zeiss Axovert S100TV microscope operated with IPLab software and a SensiCam QE CCD camera). The ratio of DNA bases to dye molecules was 6:1, and the DNA molecules were visualized using a 63× oil objective. Image acquisition times varied from 100 to 500 ms, and the interval between image collection ranged from 100 ms to 3 s. Molecules were monitored for periods of up to 25 min, shuttering (Vincent Associates Uniblitz) employed to eliminate light exposure except during image acquisition.

Circular DNA plasmids of various sizes were purchased from New England Biolabs along with restriction enzymes for cutting these plasmids into linear chains. Combinations of linearized plasmid and cavity sizes that produced useful partitioning data are given in Table 1. Tabulated radii of gyration R_{g0} are estimates of DNA's ideal or unperturbed dimensions in absence of intercalating dye; unfortunately, sample quantities were insufficient for measurement of actual radii of gyration R_g, expected in all cases to exceed R_{g0} by less than 50%. Cavity diameters, measured by optical microscopy, were nearly indistinguishable from the diameters of templating colloid(s). Under all conditions listed in Table 1, R_{g0} is much less than the larger diameter D_1 or the smaller diameter D_2 of the cavities in which partitioning was examined. Following past practice, we view confinement under such conditions as "weak" or "moderate".

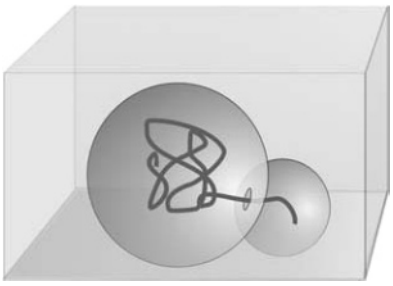

Figure 1. Schematic of two-cavity confinement for unequal size cavities.

A second round of experiments explored polymer partitioning under "strong" confinement conditions, those for which R_{g0} approaches or exceeds cavity diameter. A single DNA (48 502 bp, R_{g0} = 520 nm) was examined in a two-dimensional hexagonally packed monolayer of interconnected, equal-sized cavities (diameter = 920 nm). Difficulty inserting DNA into cavities at strong confinement underscored the change of protocols from the first round of experiments. Valid realizations are much more abundant in cavity monolayers than in isolated cavity pairs.

Results

Isolated Cavity Pairs: Weak and Moderate Chain Confinement. We previously reported single molecule visualization of polymer diffusion within two-dimensional cavity arrays made by colloidal templating.[21] The focus now turns to thermodynamics rather than dynamics. The different objective favors pore geometries that impose two regions of unequal confinement connected by a passage that allows rapid chain interchange. From experience with cavity arrays, we envisaged that evaporative deposition of highly dilute, bidisperse colloidal beads would drive at least a few mismatched beads to pair on a substrate, creating templates for isolated, asymmetric cavity pairs. From the same experience, we anticipated that each isolated cavity pair would host a round interconnecting hole. We thus chose the target geometry sketched in Figure 1. Even at the outset, some difficulties could be anticipated with this approach. First, the desired cavity pairs will be extremely sparse, and second, only a small fraction of these pairs will likely contain a DNA molecule. The overall success rate will inevitably be low. We hoped that rapid scanning by optical microscopy would lead us to the few cavity pairs of appropriate configuration.

Each consideration of the previous paragraph was borne out by actual experiment. Properly trapped DNA chains could be identified and then imaged as Brownian motion "rattled" the chains within and between cavities. Figure 2 shows a sequence of six selected images illustrating the rattling of a 7249 bp DNA between 1400 ad 608 nm diameter cavities. In the 4 min realization from which these frames were extracted, the molecule jumped from the large to the small cavity, where the molecule resided for several seconds before jumping back. DNA configurations are partially resolved in the large cavity but not elsewhere. Spatial resolution of DNA configuration is mainly limited by fluctuations over the finite period of image capture. Resolution in the small cavity and in the region of the interconnecting

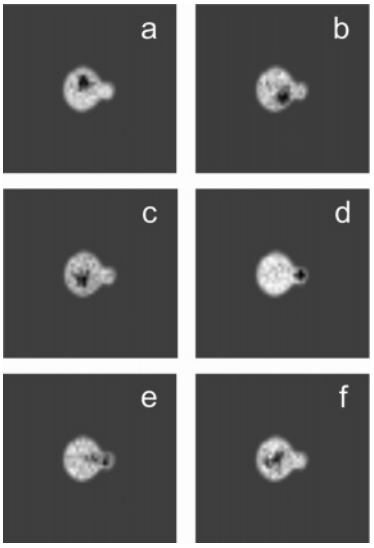

Figure 2. Six frames of 7249 bp DNA partitioned dynamically between 1400 and 608 nm diameter cavities. Each frame overlaps visible and fluorescence images. In these nonsequential frames, DNA appears as a diffuse blackened speckle or streak against the lighter background of the cavities; the chain is better resolved when the fluorescent image is colorized. Optical effects exaggerate the size of interconnecting hole. In frame d, the DNA is fully confined to the smaller cavity; in frame e, the DNA bridges.

hole is reduced by refraction from cavity walls. Of the hundreds of frames collected in this particular sequence, only one (frame e) reveals an obvious bridging configuration. Other frames offer no indication that segments of a confined chain even partially fingered into the opposite cavity, although a small, highly transient fraction of penetrated segments could well escape detection.

Optical and electron microscopies revealed good replication of polystyrene beads by open spherical cavities, but little information could be garnered about cavity-to-cavity interconnecting holes. For equal-sized cavities in a monolayer, holes were nearly circular, their diameters roughly 20% of that for the two contacting beads. For pairs of unequal-sized cavities, holes could not be imaged accurately due to their scarcity and awkward geometry. The contact of bead with planar substrate can be viewed as the limit of asymmetric bead contact. Holes created by this asymmetric contact possess a diameter about 30−35% of that of the contacting bead. From the similar outcomes at the two limits, we deduce that hole diameter for unequal cavity pairs lies around 30−35% of the small bead diameter. It must be emphasized, however, that to the extent that DNA confinement is not significantly disturbed, hole diameter is unimportant to interpretation of equilibrium partitioning. Holes are needed only to achieve rapid thermal equilibration of polymer between neighboring cavities. If our deduction about their size is correct, holes were large enough to admit DNA kinks and folds.

Each molecular realization was tracked until fluorescence bleaching led to significant loss of image quality, between 2 and 25 min, a period dependent on the size of the chain, the cavity geometry, and the illumination protocol needed to image chain location. Asserting the principle of ergodicity, the cavity-to-cavity partition coefficient K_p is the ratio of times spent in small and big cavities divided by the corresponding ratio of cavity volumes. This coefficient equals the ratio of partition coefficient K_1 and K_2 for the two separated cavities. Since cavity-to-cavity jumps were infrequent, averaging over multiple realizations was necessary to improve statistical accuracy in K_p. Where confinement remained weak or moderate, as was the case for all isolated cavity pairs, the rare frames displaying bridging configurations were ignored. In remaining frames of an image sequence, molecules could be unambiguously assigned to one of the two cavities. Defining ΔS_p as the confinement entropy difference between cavities, $K_p = \exp(\Delta S_p/k)$. The Gaussian chain theory predicts

$$\ln K_p = \ln \frac{K_2}{K_1} = (2/3)\pi^2 Lb(1/D_1^2 - 1/D_2^2) \qquad (2)$$

where L and b are the contour and Kuhn lengths of the polymer, respectively. The final expression accounts only for the first term of expansions for K_1 and K_2 (the full expansion is given as eq 2 in ref 5), but at confinement conditions encountered for isolated cavity pairs, higher terms were insignificant.

Although sampling errors in K_p diminished as more cavity-to-cavity jumps were registered, a single molecule method cannot achieve the precision of a method sensitive to the full ensemble. The number of jumps convolutes the abundance of realizations with the magnitude of K_p. We imposed the minimum requirements of two realizations and four jumps, thereby eliminating many sought-after parameter combinations. Data passing these requirements span the interval $0.01 < K_p < 1.0$ for a disparate set of cavity pairs and DNA sizes. Fortunately, this interval corresponds to the confinement conditions of greatest relevance to polymer separation methods. Values of K_p are listed in the last column of Table 1.

In comparing experiment to theory, an important consideration is the impact of intercalating dye on the physical properties of DNA. According to literature, at the labeling condition chosen, TOTO-intercalated DNA is about 33% longer than native DNA.[22,23] The literature is less clear about the effect of the dye on DNA stiffness.[22,24] We used analytical centrifugation in the velocity mode to measure the friction coefficient of single persistence length, TOTO-intercalated DNA. Applying the wormlike chain model[25] and assuming dye-insensitive specific volume and hydrodynamic radius, the measurement yielded $b = 50 \pm 22$ nm. For native DNA, $b = 100$ nm, demonstrating that dye intercalation, as performed here, reduces chain stiffness. A related issue is the potential loss of chain stiffness as single strand nicks form under illumination of the microscope. At high light levels, chain breakage occurs frequently, presumably because of the development of closely spaced nicks on opposite strands of the double helix. At the lower light levels chosen for this study, breakages are rare, and DNA behavior appears steady in time.

Employing dye-corrected values for L and b, Figure 3a plots the measured K_p against the theoretical prediction of eq 2. The 95% confidence interval error bars plotted in the figure and listed in Table 1 manifest random sampling errors, which are substantial for the experimental conditions providing few jumps. The ratios of R_{g0} to D_1 and D_2 ranged from 0.072 to 0.21 and 0.11 to 0.37, respectively, and the ratio of D_1 to D_2 ranged from 1.0 to 2.3. Both small and large cavity diameters varied sufficiently to illustrate both weak and moderate chain confinement, corresponding to chains trapped in

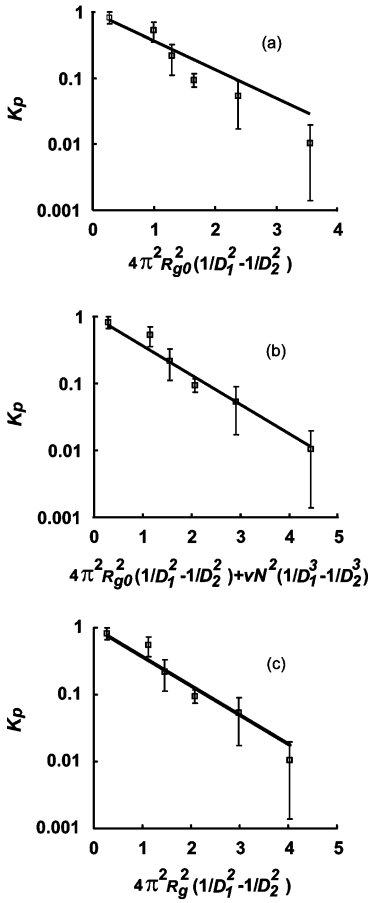

Figure 3. Experiment compared to theory for the cavity-to-cavity partition coefficient K_p: (a) Gaussian chain theory and (b, c) excluded-volume theory. In (b), correction for excluded volume is made by adding to the abscissa of (a) a term manifesting segment−segment repulsion. In (c), correction for excluded volume is made by replacing the unperturbed radius of gyration R_{g0} of (a) with a fitted scaling form for the perturbed radius of gyration R_g.

much larger or comparably sized pores, respectively. With no adjustable parameters, good agreement is demonstrated between experiment and Gaussian chain theory for the interval $0.3 < K_p < 1.0$, but agreement worsens at smaller K_p, where the theory systematically overpredicts the measurements. We conclude that the theory correctly identifies a complex variable combination that controls K_p when confinement conditions are weak and not too dissimilar between cavities.

The discrepancy between theory and experiment at small K_p can be understood in terms of segmental excluded volume. The enhanced segment density in the small cavity emphasizes excluded-volume interactions, lowering K_p. Modeling this "crowding" effect via an approximate mean-field or Flory-type argument adds a contribution to ΔS_p of the form[26]

$$\Delta S'_p \sim vN^2(1/D_1^3 - 1/D_1^3) \quad (3)$$

where v, a measure of excluded-volume interaction strength, is proportional to the segment−segment binary cluster integral. The mean-field argument supposes that segments distribute themselves uniformly throughout the cavity interior, only a zero-order approximation to the actual distribution. Further, the argument assumes that excluded volume makes only an additive correction to ΔS_p, again a crude approximation. Onsager evaluated the binary cluster integral for a pair of charged cylinders,[27] and numerous successful models for DNA virial coefficients and single chain dimensions have incorporated his result.[8,28] For confinement of cylindrical segments in a large spherical cavity, Onsager's result can be written $v = 1.5b^2d_{eff}$, where d_{eff} is the effective DNA backbone diameter. For 0.035 molar 1:1 electrolyte, parameters characterizing the buffer of this study, Stigter solved the nonlinear Poisson model for a DNA segment to find $d_{eff} = 9$ nm. Substituting Stigter's value into Onsager's expression, we find $v = 34\,000$ nm^3. Figure 3b presents a comparison of experiment measurements to excluded-volume-extended theory. Without any fitting parameters, agreement is excellent throughout, and the previous discrepancy at small K_p is resolved.

Several confinement studies[2,12,29,30] have treated excluded volume differently, replacing $Lb/6$ of Casassa's formula by R_g^2, the squared radius of gyration of the unconfined polymer in the presence of excluded volume. Conceptually, the excluded-volume correction to K_p is thereby implemented prior to pore entry rather than afterward. Unfortunately, given the minute sample amounts available, R_g is not available for our systems. If we adopt the usual scaling relationship for R_g, i.e., $R_g = aN^{3/5}$, and apply the alternative excluded-volume treatment with a as a fitting parameter, theory and experiment mesh about as well as in Figure 3b, a comparison shown in Figure 3c. Neither treatment of excluded volume is entirely satisfactory from the theoretical perspective, but the good agreement both offer for experimental data convincingly demonstrates the substantial impact of excluded volume on K_p when this parameter is less than 0.3.

A correction for finite chain/segment length does not seem necessary to improve theory−experiment agreement. However, without theory or simulation results available for a semiflexible chain in a spherical cavity, we have no direct means to confirm this conclusion rigorously. Confinement in closed cavities of the type examined here, those which fully encase trapped chains, differs significantly from confinement in unbounded slit or cylinder pores, which offer unlimited chain stretching in one or more directions.[15,26] For the latter geometries, de Gennes showed through the notion of "blobs" that the scaling relationship of eq 1 could easily be modified to account for excluded volume;[3] the premise of the scaling argument, that $\Delta S_c \sim N$, does not hold in closed cavities for chains with excluded volume. The argument fails because one cannot depict the chain as a sequence of independent blobs, each with a size comparable to the local pore dimension. Unlike the experiments to be described next, confinement levels in these first partitioning experiments were always low enough to maintain the segment density of the confined polymer below the bulk overlap concentration. In terms of their physical dimensions, chains occupied volume fractions varying from 4×10^{-6} to 4×10^{-4}; in terms of their larger, electrostatically defined dimensions, chains occupied volume fractions varying from 5×10^{-5} to 6×10^{-3}.

Cavity Pairs in a Hexagonal Cavity Array: Strong Chain Confinement. In the second partitioning experiments, the propensity of a single, large, and strongly confined DNA molecule to bridge or straddle between two equal-sized cavities was explored. These experiments focused on just one DNA species trapped in cavities of just one size, the polymer's radius of

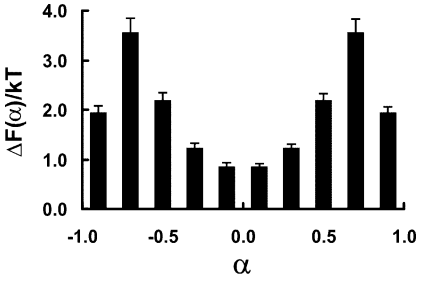

Figure 4. Free energy histogram for configurations adopted by 48 502 bp DNA in a pair of 920 nm diameter cavities. The asymmetry parameter α reflects the split of the chain segments between cavities. Cavities with $\alpha = 0$ representing configurations which exactly balance the chain between cavities and $\alpha = \pm 1$ representing configurations with the chain localized to a single cavity.

gyration selected to exceed the cavity radius. The latter condition was observed to change confinement behavior abruptly from that described already. The immediately obvious difference is dominance of bridging configurations.

To quantify these configurations, we defined an asymmetry parameter α to designate how chain segments split among cavities. Referencing the cavities by subscripts 1 and 2, $\alpha = (I_2 - I_1)/(I_2 + I_1)$, where I_i is the integrated fluorescence intensity of cavity i. We established that for a single confined chain the total intensity $I_2 + I_1$ is constant, a fact confirming linear response of integrated intensity with respect to number of segments. As a polymer moved from complete confinement in cavity 1 to complete confinement in cavity 2, α shifted from −1 to +1, passing through 0 when the segment split was even. Because observing strong confinement in isolated cavity pairs proved problematical (we never observed even a single realization for the polymer/cavity combination we now discuss), behavior at this condition was studied in hexagonally closed-packed cavity arrays, which produce abundant realizations. Each cavity in an array has six interconnecting holes, which combine to perturb idealized spherical confinement more so than do the single holes of isolated cavity pairs. Although observed regularly, the minority of polymer configurations involving three or more cavities was simply ignored. Statistical analysis provided the function $P(\alpha)$, the probability of a particular briding configuration. By definition, $P(\alpha)$ is symmetric about $\alpha = 0$. The Boltzmann distribution transforms $P(\alpha)$ to $\Delta F(\alpha)$, the free energy distribution for two-cavity configurational states.

Figure 4 displays $\Delta F(\alpha)/kT$ for 48 502 bp DNA trapped in 920 nm diameter cavities, a polymer/cavity combination producing frequent bridging. Indeed, the figure demonstrates that the equally split configuration, $\alpha = 0$, is the one of lowest free energy. Slightly less favored, by about 1 kT, are the fully asymmetric configurations, $\alpha = \pm 1$, that place the molecule wholly in one of the two cavities. The $\alpha = \pm 1$ configurations are separated from the $\alpha = 0$ configuration by an energy barrier of about 3 kT. The curve of Figure 4 demonstrates that a strongly confined polymer with excluded volume must overcome a doubly peaked energy barrier to move from one cavity to another. Smaller polymers, such as those analyzed earlier, must only surmount a singly peaked energy barrier at $\alpha = 0$, making bridging configurations unstable. Consequently, these configurations were relatively rarer than for larger chains and also more fleeting. These characters prevented us from developing meaningful free energy histograms with a single peak. Nonetheless, the observed dynamics unequivocally reveals singly peaked energy barriers for smaller chains; i.e., these chains do not pause at all as they pass through $\alpha = 0$. For 920 nm diameter cavities, the crossover DNA size characterizing the switch from doubly to singly peaked barrier seems to about 20−25 kbp, roughly corresponding to R_g equal to cavity radius.

The origins of stable bridging configurations are clear. As a DNA molecule traverses from one cavity to another, the intervening hole "pinches" the molecule's midsection, costing it configurational entropy. The molecule can avoid this penalty by escaping to a single cavity. But for a strongly confined chain with excluded volume the escape also has its cost, as single cavity configurations increase repulsive segmental interactions. These interactions are weakest in the symmetric, pinched configuration, where the spreading of segments over the full accessible volume minimizes crowding. The excluded-volume effect is negligible at low molecular weight, allowing pinched configurations to be avoided, but dominates at high molecular weight, where pinched configurations are not just tolerated but favored. For chains with excluded volume, bridging configurations first become stable when R_g exceeds about the cavity radius. Thus, from a different perspective, bridging can be viewed as a mechanism for excluded-volume chains to evade strong confinement.[31] Gaussian chains also bridge, but only due to fluctuations. Since the various energies are all of order kT, simulations will be necessary to explore tradeoffs fully.

Conclusions

Although an old topic, polymer partitioning has not previously been scrutinized by experiment in such a detailed manner. This work pioneers the study of partitioning in highly ordered environments—a long-standing problem to the polymer separations community—and introduces the quantitative measurement of polymer partition coefficients by direct visualization—a task made feasible by recent innovations in single molecule imaging. In combination, these contributions point toward a rigorous, molecule-level assessment of both classic and new partitioning theories. Such assessments are needed as new nanotechnologies, with pore spaces optimized for separation efficiency and speed, replace conventional disordered polymer separation media.

The partitioning behaviors reported here for flexible polymers are consistent with both theoretical expectations and past measurements. As the single molecule method improves so as to produce more realizations in a greater variety of confinement geometries, many nuances of partitioning should become open for study for the first time. The current results highlight complications associated with excluded volume, a property of relevance to nearly all applications of partitioning. Additional complications, especially those inherent to a separation environment (flow, external fields, and adsorption), are now being probed.

Acknowledgment. This research was supported by the National Science Foundation-sponsored Materials Research Science and Engineering Center at the University of Massachusetts Amherst.

References and Notes

(1) Daoud, M.; de Gennes, P. G. *J. Phys. (Paris)* **1977**, *38*, 85−93.

(2) Teraoka, I. *Prog. Polym. Sci.* **1996**, *21*, 89−149.
(3) de Gennes, P. G. *Scaling Concepts in Polymer Physics*; Cornell University Press: Ithaca, NY, 1979.
(4) Casassa, E. F.; Tagami, Y. *Macromolecules* **1969**, *2*, 14−26.
(5) Casassa, E. F. *J. Polym. Sci., Part B: Polym. Lett.* **1967**, *5*, 773−778.
(6) Giddings, J. C.; Kucera, E.; Russell, C. P.; Myers, M. N. *J. Phys. Chem.* **1968**, *72*, 4397−4408.
(7) Davidson, M. G.; Suter, U. W.; Deen, W. M. *Macromolecules* **1987**, *20*, 1141−1146.
(8) Odijk, T. *Macromolecules* **1983**, *16*, 1340−1344.
(9) Teraoka, I.; Langley, K. H.; Karasz, F. E. *Macromolecules* **1992**, *25*, 6106−6112.
(10) Muthukumar, M. *J. Chem. Phys.* **2003**, *118*, 5174−5184.
(11) Limbach, K. W.; Nitsche, J. M.; Wei, J. *AIChE J.* **1989**, *35*, 42−52.
(12) Cifra, P.; Bleha, T. *Macromolecules* **2001**, *34*, 605−613.
(13) Tsonchev, S.; Coalson, R. D. *Chem. Phys. Lett.* **2000**, *327*, 238−244.
(14) Jaeckel, A.; Dayantis, J. *J. Phys. A: Math. Gen.* **1994**, *27*, 2653−2667.
(15) Jaeckel, A.; Dayantis, J. *J. Phys. A: Math. Gen.* **1994**, *27*, 7719−7731.
(16) Colton, C. K.; Lai, C. J.; Satterfield, C. N. *AIChE J.* **1975**, *21*, 289−298.
(17) Satterfield, C. N.; Colton, C. K.; Turckheim, B. D.; Copeland, T. M. *AIChE J.* **1978**, *24*, 937−940.
(18) White, J. A.; Deen, W. M. *Macromolecules* **2000**, *33*, 8504−8511.
(19) Teraoka, I. *Macromolecules* **1996**, *29*, 2430−2439.
(20) Bezrukov, S. M.; Vodyanoy, I.; Brutyan, R. A.; Kasianowicz, J. J. *Macromolecules* **1996**, *29*, 8517−8522.
(21) Nykypanchuk, D.; Strey, H. H.; Hoagland, D. A. *Science* **2002**, *297*, 987−990.
(22) Bordelon, J. A.; Feierabend, K. J.; Siddiqui, S. A.; Wright, L. L.; Petty, J. T. *J. Phys. Chem. B* **2002**, *106*, 4838−4843.
(23) Perkins, T. T.; Smith, D. E.; Larson, R. G.; Chu, S. *Science* **1995**, *268*, 83−87.
(24) Smith, D. E.; Perkins, T. T.; Chu, S. *Macromolecules* **1996**, *29*, 1372−1373.
(25) Yamakawa, H.; Fujii, M. *Macromolecules* **1973**, *6*, 407−415.
(26) Grosberg, A. Y.; Khohlov, A. R. *Statistical Physics of Macromolecules*; American Institute of Physics: New York, 1994.
(27) Onsager, L. *Ann. N.Y. Acad. Sci.* **1949**, *51*, 627−659.
(28) Stigter, D.; Dill, K. A. *Macromolecules* **1995**, *28*, 5325−5337.
(29) Cifra, P.; Bleha, T.; Romanov, A. *Polymer* **1988**, *29*, 1664−1668.
(30) Bleha, T.; Cifra, P.; Karasz, F. E. *Polymer* **1990**, *31*, 1321−1327.
(31) Kong, C. Y.; Muthukumar, M. *J. Chem. Phys.* **2004**, *120*, 3460−3466.

MA048062N